Controlling the Lithiation-Induced Strain and Charging Rate in Nanowire Electrodes by Coating

Li Qiang Zhang,[§,¶,#] Xiao Hua Liu,[†,#] Yang Liu,[†] Shan Huang,[‡] Ting Zhu,[‡,*] Liangjin Gui,[⊥] Scott X. Mao,[§] Zhi Zhen Ye,[¶] Chong Min Wang,[∥] John P. Sullivan,[†] and Jian Yu Huang[†,*]

[†]Center for Integrated Nanotechnologies (CINT), Sandia National Laboratories, Albuquerque, New Mexico 87185, United States, [‡]Woodruff School of Mechanical Engineering, Georgia Institute of Technology, Atlanta, Georgia 30332, United States, [§]Department of Mechanical Engineering and Materials Science, University of Pittsburgh, Pittsburgh, Pennsylvania 15261, United States, [⊥]State Key Laboratory of Automotive Safety and Energy, Department of Automotive Engineering, Tsinghua University, Beijing 100084, People's Republic of China, [∥]Environmental Molecular Sciences Laboratory, Pacific Northwest National Laboratory, Richland, Washington 99354, United States, and [¶]State Key Laboratory of Silicon Materials, Department of Materials Science and Engineering, Zhejiang University, Hangzhou, 310027, People's Republic of China. [#]These authors contributed equally to this work.

ABSTRACT The advanced battery system is critically important for a wide range of applications, from portable electronics to electric vehicles. Lithium ion batteries (LIBs) are presently the best performing ones, but they cannot meet requirements for more demanding applications due to limitations in capacity, charging rate, and cyclability. One leading cause of those limitations is the lithiation-induced strain (LIS) in electrodes that can result in high stress, fracture, and capacity loss. Here we report that, by utilizing the coating strategy, both the charging rate and LIS of SnO_2 nanowire electrodes can be altered dramatically. The SnO_2 nanowires coated with carbon, aluminum, or copper can be charged about 10 times faster than the noncoated ones. Intriguingly, the radial expansion of the coated nanowires was completely suppressed, resulting in enormously reduced tensile stress at the reaction front, as evidenced by the lack of formation of dislocations. These improvements are attributed to the effective electronic conduction and mechanical confinement of the coatings. Our work demonstrates that nanoengineering the coating enables the simultaneous control of electrical and mechanical behaviors of electrodes, pointing to a promising route for building better LIBs.

KEYWORDS: lithium ion battery · lithiation-induced strain · charging rate · coating · tin oxide · *in situ* transmission electron microscopy

Tin oxide (SnO_2) represents one of the most promising anode materials to replace the carbonous anodes for lithium ion batteries (LIBs), with a high theoretical capacity of 781 mAh/g, and demonstrated reversible capacity exceeding 500 mAh/g.[1−3] Unlike the small volume change (usually less than 10%) in an intercalation anode such as graphite, huge volume change inevitably occurs in Sn- or Si-based alloying anodes with higher capacity.[4−6] Such volume change generates large lithiation-induced strain (LIS) and stress up to 10 GPa[7] and causes fracture and pulverization of the electrodes.[6,8] To mitigate these adverse effects for better capacity retention, several measures could be applied, for instance, by making hollow or porous nanostructures to adapt the volume change,[1,9] adding an elastomeric binder as a buffer,[10] or encapsulating the high-capacity material in a robust sheath such as carbon nanotubes.[1,3,11,12]

On the other hand, operating a LIB depends critically on a concordant transport of electrons and ions through multicomponents of the battery in addition to the mechanical stability of the electrodes during charging and discharging.[2,5,9,13−17] Since the cathode and anode materials used for LIBs are mostly poor electron conductors,[18,19] it is a common practice to incorporate conductive materials, such as carbon,[1,20−22] into the electrode to improve the electrical conductance.[23,24] In the case of SnO_2, it is known as a wide band gap semiconductor (E_g = 3.6 eV) with poor electronic conductivity.[9] In contrast, the electrodes of SnO_2 with the carbon coating have shown high capacity, good rate performance, and improved cyclability.[1,3,11,12] For example, it was reported that carbon-coated SnO_2 nanowires or nanorods show increased capacitance and cyclability as compared to the noncoated ones, which is attributed to the increased electrical conductivity and mechanical restraining effect of the carbon coating.[3,12] However, consequences of such a coating on other key aspects of lithiation-related behaviors have not been studied in a controlled fashion.[25,26] For example, it is far from clear how such a conductive coating layer will affect the electrochemically induced mechanical response, which is a critical factor limiting the capacity and cyclability of LIBs.

* Address correspondence to jhuang@sandia.gov, ting.zhu@me.gatech.edu.

Received for review February 24, 2011 and accepted May 4, 2011.

Published online May 04, 2011
10.1021/nn200770p

Here we report an *in situ* nanobattery study of the dramatic effects of carbon, aluminum, and copper coatings on both the lithiation rate and mechanical confinement associated with the electrochemically induced volume changes in a model system of SnO_2 nanowires. A schematic illustration of the carbon-coated SnO_2 single nanowire battery is shown in Figures S1 in the Supporting Information. A few SnO_2 nanowires were attached to an aluminum rod with conductive silver epoxy, while a bulk $LiCoO_2$ film on an Al foil served as the cathode. One drop of the ionic liquid electrolyte [ILE, 10 wt % lithium bis-(trifluoromethylsulfonyl)imide (LiTFSI) dissolved in 1-butyl-1-methylpyrrolidinium bis(trifluoromethylsulfonyl)imide (P_{14}TFSI)] was placed on the surface of $LiCoO_2$ film as the electrolyte.[7] A constant potential of −3.5 V was applied to the SnO_2 nanowire against $LiCoO_2$ upon charging and 0 V upon discharging.

RESULTS AND DISCUSSION

Figure 1 shows the morphological evolution of a SnO_2 nanowire without carbon coating during charging. The pristine SnO_2 nanowire was initially straight and uniform in diameter (Figure 1a). As the reaction fronts (marked by the red triangles) propagated from the right to the left, the SnO_2 nanowire swelled and bent (Figure 1a−j). The overall structural evolution of the pristine SnO_2 was reported in detail in a previous publication,[7] which was characterized by a total volume expansion of ∼240% with ∼45% radial and ∼60% axial elongation. The charging process was slow, and the reaction front migrated at an average speed of ∼0.6 nm/s. Figure 1k−p shows the typical microstructure change of a SnO_2 nanowire during lithiation. The pristine SnO_2 nanowire was single-crystalline (Figure 1k−m), which turned to gray-contrasted amorphous (Figure 1n) after lithiation. The electron diffraction pattern (EDP) from the lithiated part confirmed the formation of amorphous Li_2O, Sn, and Li_xSn phases (Figure 1p). The predominant feature in the EDP from lithiated SnO_2 nanowires was the two broad bands centered at the positions corresponding to the {101} (d = 3.959 Å) and {110} (d = 2.349 Å) planes of the hexagonal $Li_{13}Sn_5$ phase (JCPDS# 29-0838). The lithiation should proceed in two steps: (1) $4Li^+ + SnO_2 + 4e^- \rightarrow 2Li_2O + Sn$; and (2) $Sn + x\,Li^+ + xe^- \leftrightarrow Li_xSn$ ($0 \leq x \leq 4.4$).[7] The volume expansion after lithiation was obvious in both the axial and radial directions (Figure 1a−j,n). As long as the radial expansion was obvious, a Medusa zone with high density dislocations was observed in the reaction front due to the high local stress (Figure 1n), which developed due to the large mismatch between the reacted and nonreacted segments of the nanowire.[7]

The lithiation behavior of a carbon-coated SnO_2 nanowire was significantly different from that of the noncoated nanowires. Figure 2a−c and movie S1 of the Supporting Information show the lithiation process of a carbon-coated SnO_2 nanowire. It was seen that no detectable radial expansion occurred, but the nanowire did elongate by ∼160%. This was in contrast to the lithiation of noncoated nanowires, in which both radial expansion and axial elongation occurred. Furthermore, the reaction fronts (marked by red triangles) did not have any visible dislocations (Figure 2a−c), which was again in contrast to the noncoated SnO_2 nanowire, in which a Medusa zone containing dislocations of high density was always presented (Figure 1n). Evidenced by the position change of a particle attached to the surface of the nanowire (marked by the blue triangles), the elongation of the nanowire pushed the lithiated part into the ILE (Figure 2a−c). The reaction front migrated at a speed of 7.7 nm/s, about 10 times higher than that without carbon coating.

Figure 2d shows a typical morphology of a carbon-coated SnO_2 nanowire before lithiation. The SnO_2 nanowire was decorated with Sn particles due to the reduction of SnO_2 to metallic Sn in the carbon coating process. The carbon layer was about 5 nm thick and was amorphous (Figure 2e). The high-resolution transmission electron microscopy (TEM) image also shows the coherent interface between the embedded Sn particle and the parent SnO_2 crystal (Figure 2e), with an epitaxial relationship of $(020)_{Sn}//(110)_{SnO2}$ and $(101)_{Sn}//(001)_{SnO2}$ as revealed by the EDP (Figure 2f). Similar to the noncoated nanowires, the carbon-coated SnO_2 nanowire showed similar reaction products (Figure 2g). The detailed structural characterization of a carbon-coated SnO_2 nanowire before and after lithiation is shown in Figure S2 in the Supporting Information. During charging, the nanowire underwent amorphization process (Figure S2a−g). Upon lithiation, a small amount of tiny Sn nanocrystals was dispersed in an amorphous matrix, consistent with the EDP showing sharp diffraction rings superimposed on amorphous halos (Figure S2f); the diffraction rings could be indexed as the $Li_{13}Sn_5$ and Sn phases. After prolonged charging, the diffraction spots from SnO_2 became weaker and weaker (Figure S2e−g). The electron energy loss spectra (EELS) confirmed Li insertion into the lithiated part (Figure S2h) and the diminishing of the well-defined peaks from crystalline SnO_2 (Figure S2i).

Figure 2h-q and Figures S3 and S4 in Supporting Information show a closer view of the microstructural evolution around the reaction front for some other carbon-coated SnO_2 nanowires. The nanowires were divided into two segments with different contrasts by the reaction fronts (marked by the red triangles), corresponding to the original Sn/SnO_2 on the left and the lithiated amorphous products on the right side. In sharp contrast to the lithiation of the noncoated SnO_2 nanowires, neither radial expansion nor dislocation zone was seen in these carbon-coated nanowires. Figure S5

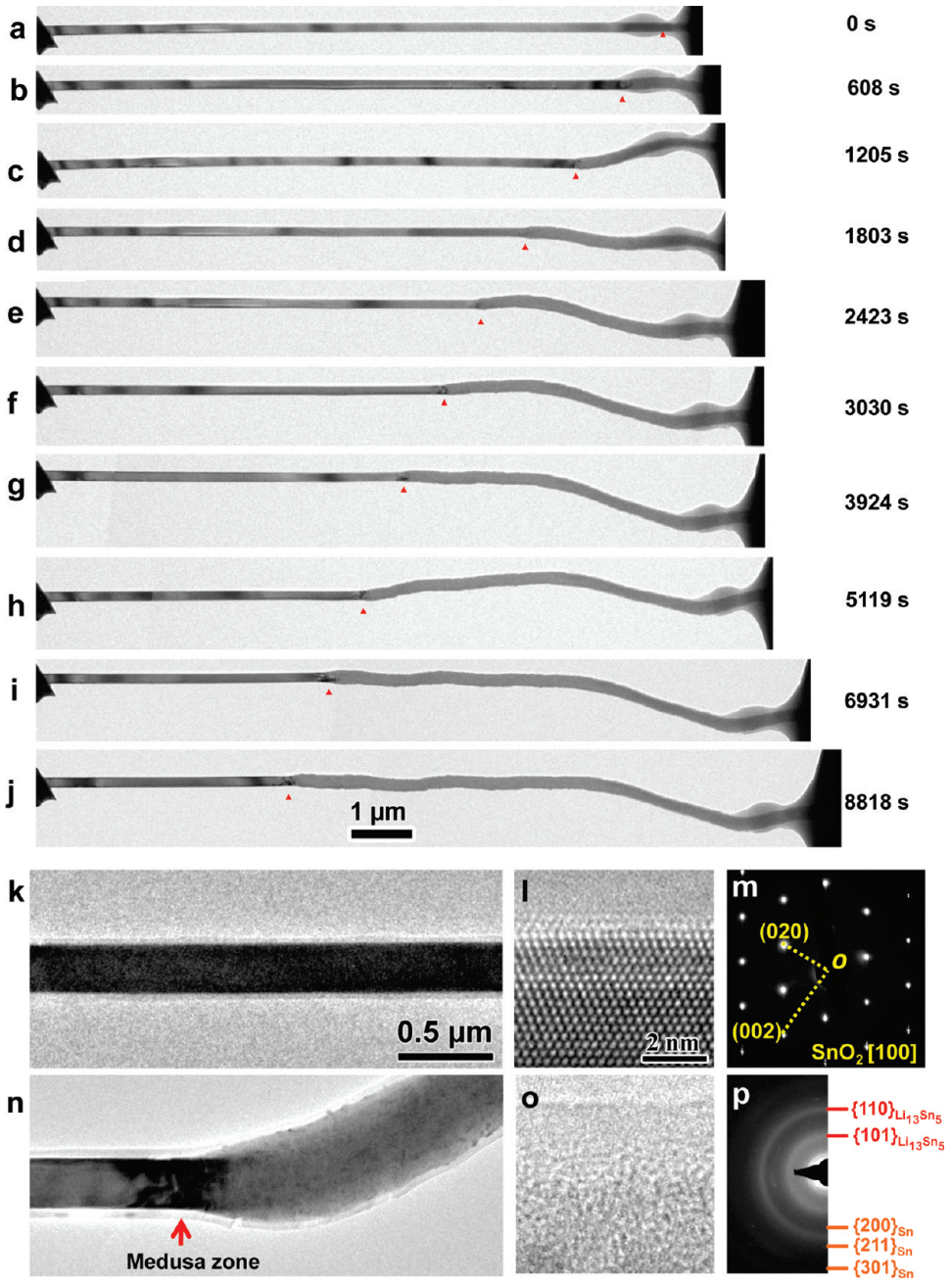

Figure 1. Charging behavior of SnO_2 nanowires without carbon coating. (a–j) Morphology evolution of a SnO_2 nanowire during charging. As the reaction front (marked by red triangles) passed by, the originally straight nanowire swelled and expanded in both radial and axial directions. The reaction fronts were heavily strained. (k–m) Microstructure of a pristine SnO_2 nanowire showing single-crystal nature. (n–p) Microstructure of the same SnO_2 nanowire after lithiation. There was obvious isotropic expansion in all directions. A strained region with visible dislocation cloud was present in the reaction front (marked by the red arrow in (n)). The EDP confirmed coexistence of amorphous Li_xSn, Sn, and Li_2O after lithiation (p). The diffraction rings from the Li_2O phase were usually very weak and thus are not marked. Note there was a thick ILE layer (not carbon coating) on the surface of the nanowire after it was immersed into the ILE (o).

shows the morphology evolution of a carbon-coated SnO_2 nanowire in the first charge/discharge cycle. After discharge, radial shrinkage was visible (Figure S5c), due to the isotropic nature of the amorphous products after lithiation. Diffraction rings from the Sn phase also showed up after discharge (Figure S5f).

Figure 3a compares the measured conductivity and lithiation rates of the carbon-coated and pristine SnO_2 nanowires. In statistics, the observed lithiation rates were 1.2 ± 0.5 and 6.6 ± 2.0 nm/s for the pristine and carbon-coated SnO_2 nanowires, respectively. On average, the reaction front of the carbon-coated nanowires moved 3–12 times faster than that of the noncoated SnO_2 nanowires. The *in situ* electrical measurements using a gold probe to contact the nanowires showed that the carbon coating improved the conductivity of

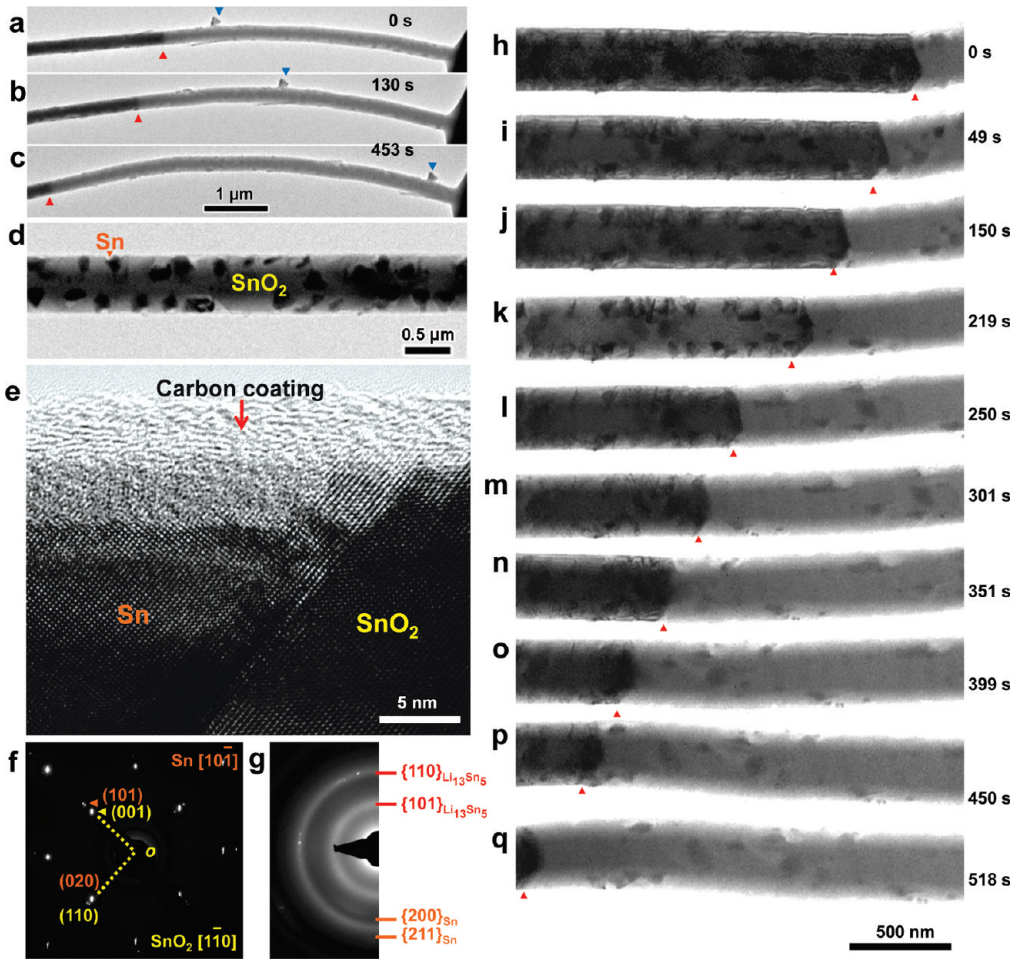

Figure 2. Microstructure evolution of SnO_2 nanowires with carbon coating during lithiation. (a−c) Lithiation with only elongation but no detectable radial expansion. The particle (marked by the blue triangles) indicated that the nanowire was continuously pushed into the ILE on the right due to elongation. (d) Low-magnification TEM image of a C-coated SnO_2 nanowire with embedded Sn nanoparticles. (e) HRTEM image of the original C-coated SnO_2 nanowire. The carbon layer was 5 nm thick and amorphous. The Sn particle formed a coherent interface with the parent SnO_2 matrix. EDPs before (f) and after (g) charging showing the phase transformation during lithiation. (h−q) High-magnification TEM images showing lithiation process of another C-coated SnO_2 nanowire. No detectable radial expansion or dislocation cloud in the reaction front existed.

the nanowires by 3−4 orders of magnitude (Figure 3a). The effects of a conformal carbon layer on the SnO_2 nanowires' lithiation include (1) higher electron transport thus faster lithiation (Figure 3b) and (2) suppressed radial expansion and exclusive elongation. As a result of the latter, no dislocation cloud was seen for the carbon-confined SnO_2 nanowires (Figure 3b). In another experiment, carbon-coated SnO_2 nanowires without the embedded Sn nanoparticles were also tested and showed similar rate enhancement and radial confinement effects (Figure S6), indicating that the rate enhancement was mainly due to the continuous carbon layer rather than the embedded but isolated Sn particles.

The suppression of radial expansion in the carbon-coated nanowire is likely to be caused by the mechanical confinement of the surface carbon layer. To assess this confinement mechanism, we have modeled the stress buildup in the coated wire by coevolving the Li diffusion and elasto-plastic deformation in the finite element simulation (see Experimental and Modeling Details). On the basis of strain measurements of the lithiated nanowires without coating, the lithiation-induced strains were taken as 45 and 60% in the radial and axial direction, respectively. The associated plastic deformation was assumed to obey the classic J_2 flow rule.[27] Figure 4a shows the simulated Li distribution and associated deformation in a carbon-coated nanowire. The simulation well captured the propagation of the lithiation reaction front in the axial direction. It also demonstrated that, due to the mechanical constraint of the carbon coating, radial expansion of the wire can be almost entirely suppressed. Moreover, in contrast to the case without coating,[7] the radial tensile stress in front of the reaction front is reduced to nearly zero in the wire, while a large radial compressive stress develops behind the reaction front (Figure 4b). The consequence of the former stress change is to reduce the driving force, and thus the possibility, of dislocation nucleation, and that of the latter is to induce plastic

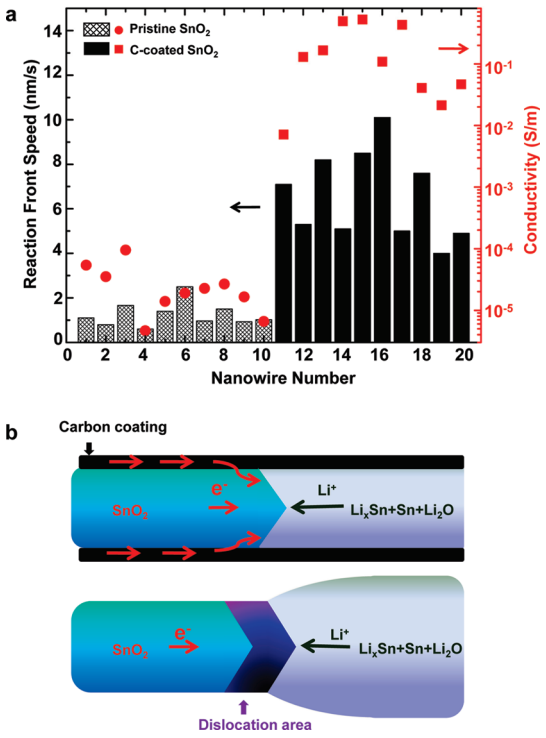

Figure 3. Comparison of lithiation behaviors of the C-coated and pristine SnO_2 nanowires. (a) Statistics of the reaction front migration speeds and conductivity. The lithiation rate was 1.2 ± 0.5 nm/s for the pristine SnO_2 nanowires (netted bars) and 6.6 ± 2.0 nm/s for the carbon-coated SnO_2 nanowires (filled bars). The conductivity of the C-coated nanowires (filled red squares) was measured to be 3−4 orders of magnitude higher than that of the pristine SnO_2 nanowires (filled circles). (b) Lithiation mechanisms. The carbon coating provided additional and predominant channels for electron transport, enhancing the charging rate. It also defined the volume expansion to occur exclusively along the longitudinal direction.

flow in the amorphous Li_xSn, leading to wire extrusion out of the free end of the carbon coating. Another effect of the mechanical confinement is to generate a hoop stress in the thin-walled cylindrical carbon coating. While the mechanical strength of the amorphous carbon coating is lower than that of perfect carbon nanotubes, the former can still fall between 25 and 90 GPa,[28,29] which should be sufficient to resist against the hoop stress-induced fracture in the coating.

One key question about the carbon coating is whether it remained intact after lithiation. Figure 4c,d shows that the continuous carbon layer was broken into tiny pieces in the axial direction after charging. Those fractures occurred due to the repeated buildup of a large axial stress, σ_z^{coat}, in the thin-walled coating when the lithiation reaction front propagates along the wire. As schematically shown in Figure 4e, σ_z^{coat} arises mainly because of the frictional shear stress at the interface between the carbon coating and the lithiated portion of the wire, which is being extruded out of the stress-free end of the coating. Assuming a constant shear stress, τ_Y, it is readily to show that $\sigma_z^{coat} \sim \tau_Y l_z/t$, where t is the thickness of the coat layer and l_z is the distance of the reaction front away from the stress-free end of the coating. As lithiation proceeds, l_z and accordingly σ_z^{coat} increase. Fracture of the coating occurs in the axial direction when σ_z^{coat} exceeds the breaking stress of the coating. As this process repeats (*i.e.*, the buildup of σ_z^{coat} and the fracture of the coating), broken segments of the surface carbon layer are left in the downstream of the lithiation reaction front (Figure 4d,e). The above scaling analysis also indicates that the stress in the coating can be controlled by tuning the thickness of the carbon layer and the interfacial shear strength. These material design aspects warrant further study for mitigating the stress and thus fracture of the coatings in the future.

The effects of a conductive coating layer on lithiation rate enhancement and modification of shape accommodation associated with volume expansion can be extended beyond the carbon material. As a demonstration, a 20 nm thick Al or Cu layer was coated onto the pristine SnO_2 nanowires, which was subjected to lithiation. Figure 5a−d and movie S2 in the Supporting Information show the lithiation of a SnO_2 nanowire partially coated with Al on the upper side. Notably, the radial expansion occurred on the side without Al coating, whereas it was suppressed on the coated side. Figure 5g shows the simulated Li distribution and deformation of the partially coated wire. It well captures the bending deformation near the reaction front, which arises because of the frictional shear stress at the interface between the coating and the lithiated wire. The EDPs confirmed the phase transformations from the Al-coated single-crystalline SnO_2 (Figure 5e) to a mixture of Sn, $Li_{13}Sn_5$, and LiAl phases (Figure 5f). This clearly proved the effect of the conductive coating on facilitating the lithiation of SnO_2 nanowires. Similarly, SnO_2 nanowires with full coverage of Al coating showed enhanced charging rate of ~9 nm/s (Figure 5h−k and Figure S7 and movie S3 in the Supporting Information). Al is a metal thus a better electron conductor than the amorphous carbon, enabling even faster lithiation rates. Such effects were also observed for SnO_2 nanowires coated with an electrochemically inert Cu layer (Figure 6). Similar to the case of a carbon coating, the Al or Cu coating was broken after lithiation but no radial expansion was observed (Figures 5h-k and 6a-e and Figure S7). Our simulations indicate that, despite the occurrence of plastic flow in the metal coating, the radial expansion of lithiated SnO_2 nanowires can still be effectively suppressed. This can be attributed to the increased flow strength and large bending resistance of the thin-walled coating. More specifically, the Al coating is about 20 nm thick in our experiments, and the yield strength of the thin coating of lithiated Al can be much higher than that of bulk Al, possibly due to both the nanometer length scale effect on dislocation starvation[30,31] and the pinning effect of Li atoms on dislocation motion. In addition, lithiation of the SnO_2 wire and Al coating needs to desynchronize around the reaction

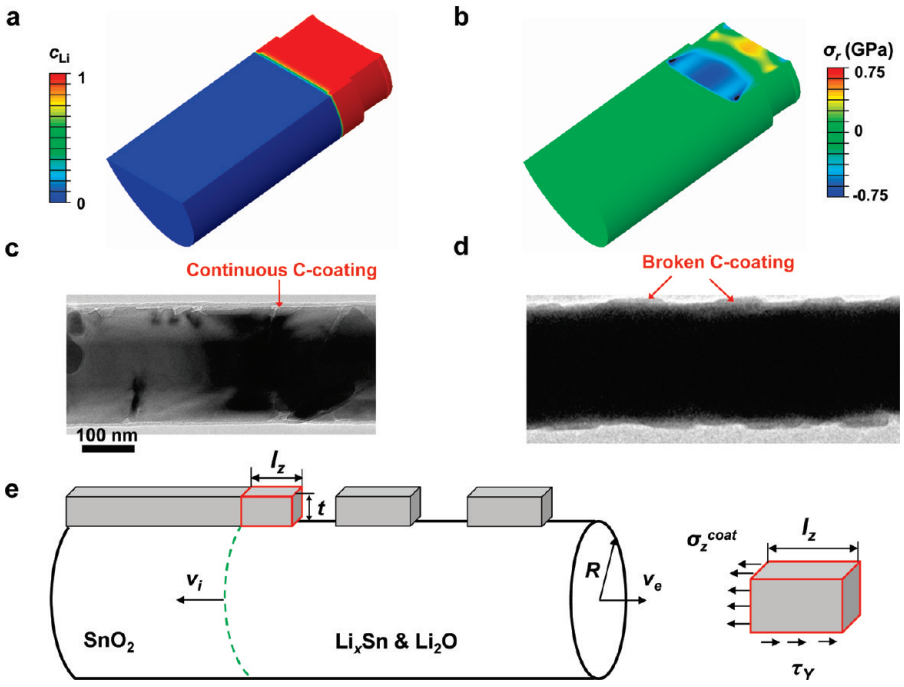

Figure 4. Simulation of Li diffusion, deformation, and stress in a carbon-coated SnO_2 nanowire. (a) Normalized Li concentration, c_{Li}, defined as the actual Li concentration divided by the Li concentration in the fully lithiated state. The lithiation reaction front is located at the interface between pristine (blue) and lithiated (red) phases. To accommodate the volume expansion, the lithiated material is extruded out of the thin-walled cylindrical carbon coating. (b) Corresponding distribution of the radial stress σ_r. (c) TEM image of a pristine SnO_2 nanowire with the continuous carbon coating and (d) that of a lithiated wire with the broken coating. (e) Schematic illustration of the development of the axial stress, σ_z^{coat}, in the carbon coating, leading to coat fracture. As lithiation proceeds, the reaction front moves to the left at a velocity v_i, and the lithiated materials behind the reaction front plastically flow in the direction opposite to v_i. A stress element of the coating is drawn on the side for a scaling analysis of σ_z^{coat}.

front, so that the lithiation-induced strain in the wire and coating would not occur simultaneously. Figure S8 shows the simulated Li distribution and deformation of the Al-coated SnO_2 nanowires. Similar to the carbon-coated wire (Figure 4), the constraint of the Al coating can largely suppress the radial expansion in the lithiated wire.

CONCLUSION

In summary, we have demonstrated the dramatic effects of the carbon, aluminum, and copper coatings on the lithiation behavior of individual SnO_2 nanowires. Compared to the noncoated SnO_2 nanowires, the coated SnO_2 nanowires can be charged at a rate 10 times higher than that of the uncoated one due to the improved electronic conductivity. More importantly, radial expansion was completely suppressed in the coated nanowires due to the mechanical confinement of the coating layers. This study demonstrated that it is possible to simultaneously control the electrochemical reaction rate and the mechanical strain of the electrode materials through carbon, aluminum, or copper coating, opening new avenues of designing better electrodes for lithium ion batteries.

EXPERIMENTAL AND MODELING DETAILS

SnO_2 Nanowire Synthesis. The SnO_2 nanowire was synthesized by a chemical vapor deposition (CVD) process using activated carbon powder (Ketjen Black, EC600JD, Akzo Nobel Corp. Japan) and SnO_2 nanoparticles (Sigma-Aldrich, particle size <100 nm) as the precursors and Au as the catalyst. The activated carbon and the SnO_2 powder were mixed at a ratio of C/SnO_2 = 1:4 (weight) using a mortar and pestle. The mixed C and SnO_2 powder was placed into a quartz boat, which was subsequently loaded into a quartz tube furnace. A Si wafer coated by a 5 nm thick sputtered Au film was located next to the quartz boat as receiving substrate. The carrier nitrogen gas (99.95% purity, 100 sccm) was flowing in the direction from the mixed powder precursor toward the Si substrate with the pressure in the tube maintained at 200 Torr. The furnace was heated at a rate of 6.5 °C/min to 800 °C and maintained at 800 °C for 6 h for the growth of the SnO_2 nanowires. Upon completion of the growth, the furnace power was shut off to allow the furnace to naturally cool. Typically, it took ~4 h for the furnace to cool from 800 °C to room temperature. The diameter of the SnO_2 nanowires ranged from several nanometers to ~1 μm, and the length of the wires ranged from several hundred nanometers to several hundred micrometers.

Carbon and Metal (Al, Cu) Coating. The carbon coating was conducted by pyrolysis of acetylene at high temperature as described here. The SnO_2 nanowires grown on a substrate were loaded in a ceramic boat and placed in the center of a quartz tube furnace. The

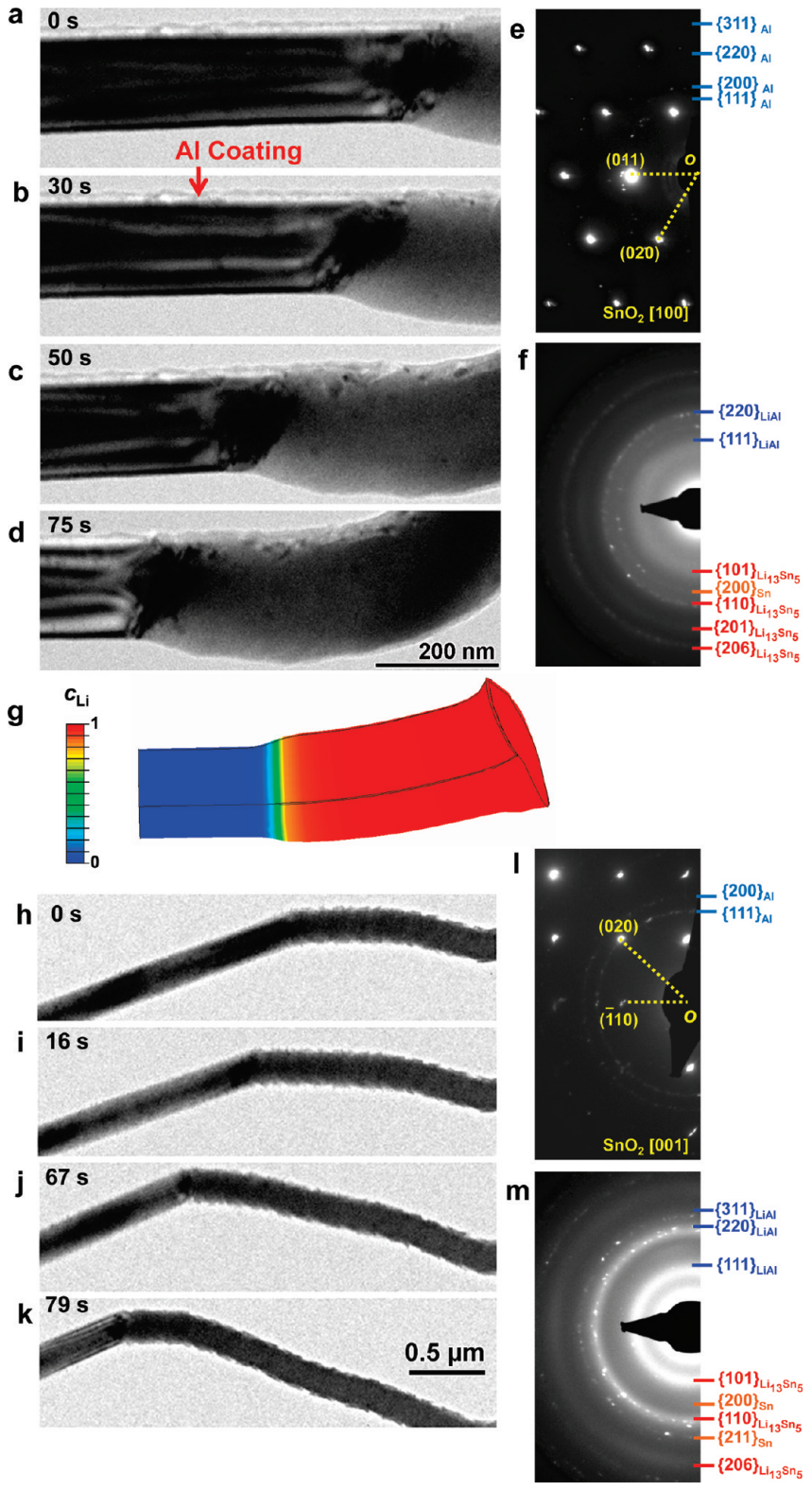

Figure 5. Lithiation behaviors of SnO_2 nanowires coated with Al layers. (a–f) Structure evolution during lithiation of a SnO_2 nanowire with one side coated with Al. The volume expansion occurred on the noncoated side but was suppressed on the coated side (a–d). (g) Simulated Li distribution and bending deformation of the partially Al-coated nanowire after lithiation. (h–m) Lithiation of a fully coated nanowire. The radial expansion was completely suppressed. The EDPs showed conversion of single-crystalline SnO_2 (e,l) to mixed amorphous phases of Sn, $Li_{13}Sn_5$, and Li_2O (f,m).

furnace was evacuated at room temperature overnight to a vacuum level less than 1 mTorr. The furnace was heated to 600 °C at a ramp of 10 °C/min. Then the precursor gas (argon/acetylene = 9:1) was introduced

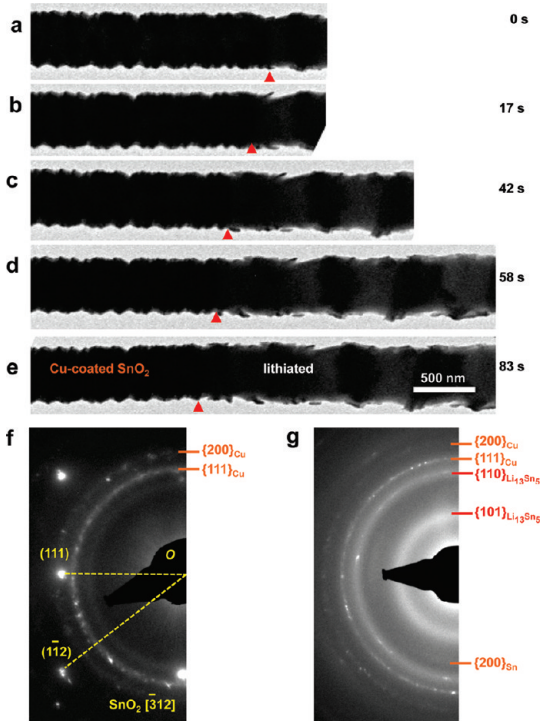

Figure 6. Lithiation behavior of a Cu-coated SnO_2 nanowire. (a−e) As the reaction front (marked by red triangles) passed by, the nanowire elongated without radial expansion due to the Cu coatings, although Cu layer was broken after lithiation. The reaction front migrated at a speed of ~6 nm/s. EDPs of the Cu/SnO_2 nanowire (f) and lithiated nanowire (g) showing the phase transformation during the lithiation.

into the furnace, and the temperature was increased from 600 to 690 °C over a 10 min period and kept at 690 °C for 30 min, during which the acetylene quickly decomposed and carbon deposited onto the surface of SnO_2 nanowires. After that, the precursor gas was stopped and the pure argon was inlet. Finally, the furnace was cooled slowly to room temperature in pure argon atmosphere, and the carbon-coated SnO_2 nanowire sample was taken out of the furnace.

The aluminum coating was conducted with an EG-1 e-beam evaporator using a high-purity Al target (purity 99.999%). For one-side coating, the sample stage was not rotated in order to receive Al flux onto only one side of the SnO_2 nanowires. For uniform and conformal coating, the sample stage was rotated to receive Al flux onto all surfaces. The conformal Cu layer was coated onto SnO_2 nanowires with a sputter using a high purity Cu target (Kurt J. Lesker, purity 99.99%).

Modeling. We have modeled the Li and stress distributions in the coated wire by coevolving the Li diffusion and elastic-plastic deformation in the finite element simulation. To simulate Li distributions, we used a nonlinear diffusion model with Li concentration-dependent diffusivities. As a first approximation, we took a simple nonlinear function of

$$D = D_0[1/(1-c) - 2\Omega c] \quad (1)$$

where D_0 is the diffusivity constant; c is the normalized Li concentration, that is, the actual Li concentration divided by the Li concentration in the fully lithiated state; Ω can be tuned to control the concentration profile near the reaction front, and we took $\Omega = 1.95$. For numerical stability, the maximum of D was capped at $300D_0$. This simple diffusion model generated a sequence of quasi-1D step-like profiles of Li distribution along the axial direction of the wire, as observed from *in situ* experiments.

To simulate the mechanical deformation, we adopted an elastic and perfectly plastic model. The increment of the total strain, $d\varepsilon_{ij}$, was taken to be the sum of three contributions[27]

$$d\varepsilon_{ij} = d\varepsilon_{ij}^{c} + d\varepsilon_{ij}^{e} + d\varepsilon_{ij}^{p} \quad (2)$$

where the increment of the lithiation-induced chemical strain, $d\varepsilon_{ij}^{c}$, is proportional to the increment of the normalized Li concentration, $d\varepsilon_{ij}^{c} = \beta_{ij}dc$. Here β_{ij} represents the expansion coefficient with nonzero direct components, and they are controlled by the atomic processes near the lithiation reaction front. Since a mechanistically based assignment of β_{ij} is beyond the scope of this work, we took β_{ij} based on the strain measurement of the lithiated SnO_2 nanowire without coating: in the cylindrical coordinated system, β_{rr} = 45%, $\beta_{\theta\theta}$ = 45%, and β_{zz} = 60%. The lithiation-induced strain in carbon coating is much smaller and was considered negligible (zeros for β_{ij}). The increment of the elastic strain, $d\varepsilon_{ij}^{e}$ in eq 2 obeys the linear elastic Hooke's law. Our elasticity model dose not account for the Li concentration dependence of Young's modulus E and Poisson's ratio ν due to the lack of experimental data. Numerical studies indicated that the results are not sensitive to the change of E and ν with Li concentration. We took E and ν from those of materials without lithiation, for SnO_2, E = 200 GPa, ν = 0.3, and for diamond-like amorphous carbon coat, E = 759 GPa, ν = 0.3. The increment of the plastic strain, $d\varepsilon_{ij}^{p}$ in eq 2 was assumed to obey the classic J_2 flow rule; namely, plastic yielding occurs when the von Mises equivalent stress, $\sigma_{eq} = (3s_{ij}s_{ij}/2)^{1/2}$, equals the yield stress σ_Y, taken as 500 MPa for SnO_2. Here $s_{ij} = \sigma_{ij} - \sigma_{kk}\delta_{ij}/3$ is the deviatoric stress; $d\varepsilon_{ij}^{p}$ is proportional to s_{ij} and can be determined by solving the boundary value problem.

We numerically implemented the above diffusion and elastic-plastic model by using the finite element package ABAQUS 6.10. The Li distribution and stress−strain fields were incrementally updated using an implicit coupled temperature displacement procedure in ABAQUS/Standard. Specifically, the lithiation-induced strain was simulated by a thermal strain approach. That is, the normalized concentration was surrogated by temperature, and the expansion coefficient β_{ij} was equivalently treated as the thermal expansion coefficient. The user material subroutine for

heat transfer (UMATHT) was programmed to interface with ABAQUS for updating diffusivities based on the current Li concentration (*i.e.*, temperature). The Li distribution was then updated and so was the increment of the elastic-plastic deformation. To simulate the axially symmetric response of the coated wire, we used the four-node axisymmetric element with thermally coupled quadrilateral, bilinear displacement, and temperature (CAX4T). The coating thickness was taken as 1/10 of the radius of the wire. The boundary conditions were taken as a constant Li flux at one end and zero traction at the outer boundary.

To accommodate the large volume expansion in the coated wire, the lithiated material was extruded out of the stress-free end of the thin-walled cylindrical coating. The extrusion process involved the complicated interfacial behaviors between the lithiated material and coating, such as large shear deformation, interfacial fracture, frictional sliding, loss of interfacial interaction between the extruded part and coating. In a first approximation, the interfacial response was simulated by using a stick-and-slip friction model implemented in ABAQUS. When the interfacial shear stress was larger than the critical value of 0.28 GPa, the interface debonded and relative sliding occurred. The friction coefficient was taken as 1 and the fraction of characteristic surface dimension as 0.01.

Acknowledgment. Portions of this work was supported by a Laboratory Directed Research and Development (LDRD) project at Sandia National Laboratories (SNL) and partly by the Science of Precision Multifunctional Nanostructures for Electrical Energy Storage (NEES), an Energy Frontier Research Center (EFRC) funded by the U.S. Department of Energy, Office of Science, Office of Basic Energy Sciences under Award Number DESC0001160. The LDRD supported the development and fabrication of platforms. The NEES center supported the development of TEM techniques, and some of the additional platform development, and fabrication and materials characterization. CINT supported the TEM capability and the fabrication capabilities that were used for the TEM characterization, in addition, this work represents the efforts of several CINT users, primarily those with affiliation external to Sandia National Laboratories. In addition, this work was performed, in part, at the Sandia–Los Alamos Center for Integrated Nanotechnologies (CINT), a U.S. Department of Energy, Office of Basic Energy Sciences user facility. Sandia National Laboratories is a multiprogram laboratory operated by Sandia Corporation, a wholly owned subsidiary of Lockheed Martin Company, for the U.S. Department of Energy's National Nuclear Security Administration under Contract DE-AC04-94AL85000. C.M.W. thanks X. Wu of PNNL for assistant on synthesis of the some of the materials used in this work. Work for C.M.W. was supported by the LDRD program of Pacific Northwest National Laboratory (PNNL) and was conducted in the William R. Wiley Environmental Molecular Sciences Laboratory (EMSL), a national scientific user facility sponsored by DOE's Office of Biological and Environmental Research and located at PNNL. PNNL is operated by Battelle for the DOE under Contract DE-AC05-76RLO1830. T.Z. acknowledges the support by NSF Grants CMMI-0758554, 0758265, and 0825435.

Supporting Information Available: Supporting figures of the experimental setup, structural characterizations, delithiation test, lithiation behavior of a C/SnO_2 nanowire, and Al-coated SnO_2 nanowires. This material is available free of charge *via* the Internet at http://pubs.acs.org.

REFERENCES AND NOTES

1. Wang, Y.; Zeng, H. C.; Lee, J. Y. Highly Reversible Lithium Storage in Porous SnO_2 Nanotubes with Coaxially Grown Carbon Nanotube Overlayers. *Adv. Mater.* **2006**, *18*, 645–649.
2. Brousse, T.; Retoux, R.; Herterich, U.; Schleich, D. M. Thin-Film Crystalline SnO_2-Lithium Electrodes. *J. Electrochem. Soc.* **1998**, *145*, 1–4.
3. Zhao, N. H.; Yang, L. C.; Zhang, P.; Wang, G. J.; Wang, B.; Yao, B. D.; Wu, Y. P. Polycrystalline SnO_2 Nanowires Coated with Amorphous Carbon Nanotube as Anode Material for Lithium Ion Batteries. *Mater. Lett.* **2010**, *64*, 972–975.
4. Larcher, D.; Beattie, S.; Morcrette, M.; Edstroem, K.; Jumas, J. C.; Tarascon, J. M. Recent Findings and Prospects in the Field of Pure Metals as Negative Electrodes for Li-Ion Batteries. *J. Mater. Chem.* **2007**, *17*, 3759–3772.
5. Chan, C. K.; Peng, H. L.; Liu, G.; McIlwrath, K.; Zhang, X. F.; Huggins, R. A.; Cui, Y. High-Performance Lithium Battery Anodes Using Silicon Nanowires. *Nat. Nanotechnol.* **2008**, *3*, 31–35.
6. Beaulieu, L. Y.; Eberman, K. W.; Turner, R. L.; Krause, L. J.; Dahn, J. R. Colossal Reversible Volume Changes in Lithium Alloys. *Electrochem. Solid State Lett.* **2001**, *4*, A137–A140.
7. Huang, J. Y.; Zhong, L.; Wang, C. M.; Sullivan, J. P.; Xu, W.; Zhang, L. Q.; Mao, S. X.; Hudak, N. S.; Liu, X. H.; Subramanian, A.; *et al. In Situ* Observation of the Electrochemical Lithiation of a Single SnO_2 Nanowire Electrode. *Science* **2010**, *330*, 1515–1520.
8. Beaulieu, L. Y.; Hatchard, T. D.; Bonakdarpour, A.; Fleischauer, M. D.; Dahn, J. R. Reaction of Li with Alloy Thin Films Studied by *In Situ* AFM. *J. Electrochem. Soc.* **2003**, *150*, A1457–A1464.
9. Lou, X. W.; Wang, Y.; Yuan, C. L.; Lee, J. Y.; Archer, L. A. Template-Free Synthesis of SnO_2 Hollow Nanostructures with High Lithium Storage Capacity. *Adv. Mater.* **2006**, *18*, 2325–2329.
10. Liu, W. R.; Yang, M. H.; Wu, H. C.; Chiao, S. M.; Wu, N. L. Enhanced Cycle Life of Si Anode for Li-Ion Batteries by Using Modified Elastomeric Binder. *Electrochem. Solid State Lett.* **2005**, *8*, A100–A103.
11. Zhang, W. M.; Hu, J. S.; Guo, Y. G.; Zheng, S. F.; Zhong, L. S.; Song, W. G.; Wan, L. J. Tin-Nanoparticles Encapsulated in Elastic Hollow Carbon Spheres for High-Performance Anode Material in Lithium-Ion Batteries. *Adv. Mater.* **2008**, *20*, 1160–1165.
12. Ji, X. X.; Huang, X. T.; Liu, J. P.; Jiang, J.; Li, X.; Ding, R. M.; Hu, Y. Y.; Wu, F.; Li, Q. Carbon-Coated SnO_2 Nanorod Array for Lithium-Ion Battery Anode Material. *Nanoscale Res. Lett.* **2010**, *5*, 649–653.
13. Arico, A. S.; Bruce, P.; Scrosati, B.; Tarascon, J. M.; Van Schalkwijk, W. Nanostructured Materials for Advanced Energy Conversion and Storage Devices. *Nat. Mater.* **2005**, *4*, 366–377.
14. Larcher, D.; Beattie, S.; Morcrette, M.; Edstroem, K.; Jumas, J.; Tarascon, J. Recent Findings and Prospects in the Field of Pure Metals as Negative Electrodes for Li-Ion Batteries. *J. Mater. Chem.* **2007**, 3759–3772.
15. Tarascon, J. M.; Armand, M. Issues and Challenges Facing Rechargeable Lithium Batteries. *Nature* **2001**, *414*, 359–367.
16. Goodenough, J. B.; Kim, Y. Challenges for Rechargeable Li Batteries. *Chem. Mater.* **2010**, *22*, 587–603.
17. Li, N. C.; Martin, C. R.; Scrosati, B. A High-Rate, High-Capacity, Nanostructured Tin Oxide Electrode. *Electrochem. Solid State Lett.* **2000**, *3*, 316–318.
18. Chung, S. Y.; Bloking, J. T.; Chiang, Y. M. Electronically Conductive Phospho-Olivines as Lithium Storage Electrodes. *Nat. Mater.* **2002**, *1*, 123–128.
19. Kang, B.; Ceder, G. Battery Materials for Ultrafast Charging and Discharging. *Nature* **2009**, 190–193.
20. Magasinski, A.; Dixon, P.; Hertzberg, B.; Kvit, A.; Ayala, J.; Yushin, G. High-Performance Lithium-Ion Anodes Using a Hierarchical Bottom-Up Approach. *Nat. Mater.* **2010**, *9*, 353–358.

21. Ng, S. H.; Wang, J. Z.; Wexler, D.; Konstantinov, K.; Guo, Z. P.; Liu, H. K. Highly Reversible Lithium Storage in Spheroidal Carbon-Coated Silicon Nanocomposites as Anodes for Lithium-Ion Batteries. *Angew. Chem., Int. Ed.* **2006**, *45*, 6896–6899.
22. Cui, L. F.; Yang, Y.; Hsu, C. M.; Cui, Y. Carbon–Silicon Core–Shell Nanowires as High Capacity Electrode for Lithium Ion Batteries. *Nano Lett.* **2009**, *9*, 3370–3374.
23. Cheng, F.; Tao, Z.; Liang, J.; Chen, J. Template-Directed Materials for Rechargeable Lithium-Ion Batteries. *Chem. Mater.* **2008**, *20*, 667–681.
24. Cui, L. F.; Ruffo, R.; Chan, C. K.; Peng, H. L.; Cui, Y. Crystalline-Amorphous Core–Shell Silicon Nanowires for High Capacity and High Current Battery Electrodes. *Nano Lett.* **2009**, *9*, 491–495.
25. Ravet, N.; Abouimrane, A.; Armand, M. From Our Readers—On the Electronic Conductivity of Phosphoolivines as Lithium Storage Electrodes. *Nat. Mater.* **2003**, *2*, 702–702.
26. Hong, J.; Wang, C. S.; Dudney, N. J.; Lance, M. J. Characterization and Performance of $LiFePO_4$ Thin-Film Cathodes Prepared with Radio-Frequency Magnetron-Sputter Deposition. *J. Electrochem. Soc.* **2007**, *154*, A805–A809.
27. Zhao, K. J.; Pharr, M.; Vlassak, J. J.; Suo, Z. G. Inelastic Hosts as Electrodes for High-Capacity Lithium-Ion Batteries. *J. Appl. Phys.* **2011**, *109*, 016110.
28. Fyta, M. G.; Remediakis, I. N.; Kelires, P. C.; Papaconstantopoulos, D. A. Insights into the Fracture Mechanisms and Strength of Amorphous and Nanocomposite Carbon. *Phys. Rev. Lett.* **2006**, *96*, 185503.
29. Espinosa, H. D.; Peng, B.; Moldovan, N.; Friedmann, T. A.; Xiao, X.; Mancini, D. C.; Auciello, O.; Carlisle, J.; Zorman, C. A.; Merhegany, M. Elasticity, Strength, and Toughness of Single Crystal Silicon Carbide, Ultrananocrystalline Diamond, and Hydrogen-Free Tetrahedral Amorphous Carbon. *Appl. Phys. Lett.* **2006**, *89*, 073111.
30. Greer, J. R.; Nix, W. D. Nanoscale Gold Pillars Strengthened through Dislocation Starvation. *Phys. Rev. B* **2006**, *73*, 245410.
31. Zhu, T.; Li, J. Ultra-Strength Materials. *Prog. Mater. Sci.* **2010**, *55*, 710–757.